Satellite Observations of Plume-Like Streaks in a Cloud Field in Canada

Lewis Grasso[a], Daniel T. Lindsey[b], Curtis J. Seaman[a], Brian Stocks[c] ,Robert M. Rabin[d]

[a]Cooperative Institute for Research in the Atmosphere (CIRA)
CIRA – 1375
Colorado State University
Fort Collins, CO 80523-1375
Lewis.Grasso@colostate.edu

[b]NOAA Center for Satellite Applications and Research
Regional and Mesoscale Meteorology Branch – CIRA
Colorado State University
Fort Collins, CO 80523-1375

[c]B.J. Stocks Wildfire Investigations Ltd.
128 Chambers Avenue
Sault Ste. Marie, ON P6A4V4, Canada

[d]NOAA/National Severe Storms Lab
Norman, OK 73072

Abstract. On the afternoon of 28 October 2013, plume-like streaks were detected by geostationary and polar orbiting satellites over eastern Ontario, Canada. These streaks were characterized by enhanced reflectivity in the visible bands and warmer brightness temperatures at 3.9 μm. These streaks were part of a low-level liquid water cloud layer. Due to the similarity of the streaks to plume-like features in marine stratocumulus caused by smoke from the stacks of ships, so-called ship tracks, a local source of emitted aerosols was suspected and subsequently identified as the burning of logging residue. This event provides further support for the ability of locally enhanced aerosol loading to alter microphysical characteristics of clouds. Ship tracks, pollution plumes from industrial burning, and pyro-cumulus are known examples of this type of interaction. In addition, the plume-like streaks could be used indirectly to identify the location of the source of the emitted particles.

Keywords: NPP-VIIRS, GOES-13, ship tracks, pollution plumes, pyro-cumulus, microphysics

1. Introduction

Space-based sensors are capable of detecting a variety of features within the atmosphere and on the surface of the Earth. Both geostationary and low Earth-orbiting satellites have been used to detect and monitor biomass burning of, for example, wildland fires, agricultural fires, and fossil fuel combustion. Such burning is a source of particulate matter that is emitted into the atmosphere (e.g., Prins and Menzel, 1992; Prins *et al*., 1998; Weaver *et al.*, 2004; Giglio *et al.*, 2003; Giglio *et al.*, 2009). A variety of consequences result from these emitted particles, including the degradation of air quality and the interaction with cloud systems.

Air quality may refer to the influence of airborne particulate matter on visibility and human health. As a result, efforts exist to monitor particulate matter (e.g., Sifakis and Iossifidis, 2014) from biomass burning (e.g., Zhang *et al.*, 2012; Kaskaoutis *et al.,* 2011) and anthropogenic sources (e.g., Cheng *et al.*, 2005; Rosenfeld, 2000). Emissions from burning may also influence cloud systems. This is done through the alteration of cloud optical thickness and particle size of liquid droplets and/or ice crystals. The increase in optical thickness and decrease in cloud particle size are due to the increase of condensation nuclei from anthropogenic sources. These extra condensation nuclei act to increase the number of cloud droplets and thus decrease the cloud droplet sizes (e.g., Twomey, 1977). Cloud enhancements caused by exhaust from the stacks of ships, so-called ship tracks, are an example in which cloud optical thickness increases and cloud liquid droplet size decreases. As a result, more solar energy is reflected back to space. This produces locally bright tracks in a layer

of marine stratocumulus as seen from satellite imagery at 0.67 μm and in the shortwave infrared at 3.9 μm (e.g., Platnick *et al.*, 2000).

Convective clouds near an active burn area may also be affected by particulates from fires. Cumulus clouds may form over or be enhanced by relatively large regions of active burning. If cumulus clouds develop deep enough, so called pyro-cumulonimbus (e.g., Fromm, 2010) may form. Such cloud systems can ingest emitted particles from wildland burning, which may result in smaller anvil ice particles and increased cloud lifetimes (e.g., Lindsey and Fromm, 2008). In addition, industrial pollution from point sources can also alter the microphysics of clouds in a way that is similar to ship tracks. Bright tracks in cloud layers downwind of industrial pollution sources have been observed and termed "pollution plumes" (e.g., Rosenfeld, 2000).

Fire detection by geostationary and/or low Earth-orbiting satellites typically requires clear sky or thin cloud conditions. Radiant energy emitted from a fire hotspot can pass through the atmosphere of the Earth and be sensed by a satellite. As a result, the phrase "direct detection" will refer to the unimpeded sensing of a surface hotspot by a satellite near 3.9 μm. In contrast, cloud cover, if thick enough, will prevent direct detection of a surface hotspot by a satellite. In this case, the phrase "indirect detection" will be used. In this paper, an example of indirect detection of biomass burning is presented.

2. Data

Two data sources were utilized for the imagery herein. They are the Geostationary Observational Environmental Satellite (GOES) -13 imager and the Suomi National Polar-Orbiting Partnership (S-NPP) Visible–Infrared Imaging Radiometer Suite (VIIRS). GOES-13 was launched in 2010 and is presently located near 75^{o} W above the equator while Suomi NPP was launched in 2011. A wide range of imagery has been captured by both GOES-13 (e.g., Hillger and Schmit, 2009) and S-NPP VIIRS (e.g., Hillger *et al.*, 2013). GOES provides imagery with better temporal resolution, while VIIRS has superior spatial and spectral resolution. On 28 October 2013 both satellites captured plume-like streaks in a low-level liquid water cloud field over eastern portions of Ontario, Canada.

Imagery from two satellite platforms will be presented. Two bands from GOES-13, bands 1 and 2, will be shown. Band 1 (0.67 μm) has a sub-satellite footprint size of 1 km while the sub-satellite footprint of band 2 (3.9 μm) is 4 km. In addition, imagery from the first four S-NPP VIIRS I-bands (0.64, 0.865, 1.61, 3.74 μm) will be shown. All I-bands have a sub-satellite footprint size of 375 m. A summary of the bands for both platforms is shown in Table 1. One last piece of information that the reader may find interesting about GOES is the over-sampling of data by the imager. In essence, data sampling is performed twice as often in the east-west direction. As a result, a second east-west set of pixels exists over a first set of east-west pixels and shifted eastward about 50 %. For completeness, over-sampling is absent for S-NPP VIIRS.

[Table 1]

3. Interpretation

At 18:53 UTC on 28 October 2013, the S-NPP satellite passed over southeastern Canada and VIIRS captured images of plume-like streaks within a layer of stratus clouds. One way to view the plume-like streaks with VIIRS imagery is through the use of a natural color composite (e.g., Hillger et al., 2013, page 1024). Bands I1 (0.64 μm), I2 (0.865 μm), and I3 (1.61 μm) are combined to produce a composite image by assigning one color to each band. In this case, band I1 is assigned the color blue, band I2 is assigned the color green, and band I3 is assigned the color red. Each color is represented by a value that ranges from 0 to 256 in an 8-bit sequence. Since each color is 8-bits and there are three colors, a total of 24-bits are then used to generate a color at one pixel in a natural color composite. Since band I1 extends into the visible spectrum, a few comments about Rayleigh scattering are warranted.

Rayleigh scattering of sun light from molecules in the atmosphere increases from 1.61 μm to 0.46 μm. In particular, Rayleigh scattering is quite significant at 0.46 μm; as a result, a process called Rayleigh correction would be necessary to apply to imagery at 0.46 μm. In contrast, Rayleigh correction has little impact for the first three I-bands that were used to create the natural color composite. Thus, no Rayleigh correction was applied to any images that were used to build a natural color composite.

A natural color composite (Fig. 1) was generated from bands I1 (0.64 μm), I2 (0.865 μm), and I3 (1.61 μm). Since bands I1, I2, and I3 are sensitive to reflection of solar energy from tops of clouds, variability of satellite measured radiances will depend primarily on the optical thickness of liquid water clouds (e.g., Platnick et al.,

2000, Fig. 1). A few brighter streaks are evident in Figure 1a within the region bounded by a white box. Brightness of the streaks can be quantified through a comparison of the reflectance values with neighboring clouds at each band. Results of the comparisons in I1, I2, and I3 indicate that, on average, reflectance values of the streaks were 13 %, 15 %, and 23 % larger, respectively, than neighboring clouds. A closer view of the streaks within the white box is displayed in Fig. 1b. Since the streaks are brighter than surrounding clouds, one can infer that the optical depth of the streaks was larger—due to a larger number of smaller cloud droplets--than the optical depth of the surrounding clouds. In addition, the streaks were brighter in bands I2 and I3 compared to band I1. As a result, the streaks may appear to have a slight yellow tint. These streaks were located about ten miles north of Lady Evelyn Smoothwater Provincial Park and about twenty miles northwest of Lake Timiskaming. For reference, this rather long and narrow lake is located to the east of the streaks and is oriented somewhat north-northwest to south-southeast and is on the border of Ontario and Quebec. Superimposed on the image in Fig. 1b are red stars that denote the latitude and longitude of the origin of each plume.

[Figure 1]

In addition to the natural color composite, S-NPP VIIRS also imaged the scene in Fig. 1 using band I4 near 3.74 μm (Fig. 2). During the daytime, measured radiances at 3.74 μm will be a combination of both emitted terrestrial energy and reflected solar energy. Due to the scattering properties of cloud liquid droplets at 3.74 μm, reflected solar energy can contribute many tens of degrees Kelvins to brightness temperatures. As a result, variability of satellite measured radiances will depend on

the sizes of cloud liquid droplets in a cloud field (e.g., Platnick et al., 2000, Fig. 1). That is, smaller cloud droplets reflect more solar radiation compared to larger cloud droplets. Similar to the appearance of the streaks in Fig. 1, in band I4 the streaks also appear warmer than the surrounding clouds. This is due to the enhanced reflection of solar energy. In particular, the average brightness temperature of the streaks was approximately 25 K warmer than nearby clouds. This result suggests that the cloud droplets were smaller in the streaks compared to cloud droplets of the surrounding liquid water cloud field.

[Figure 2]

Further evidence to support the claim that smaller cloud particles existed within the bright steaks is provided by a VIIRS retrieval of cloud top particle sizes (e.g., NPOESS ATBD, 2010). Figure 3a shows a close-up view of the cloud streaks from Fig. 1. For clarity sake, some of the bright streaks have been denoted by red line segments. In the same field of view as Fig. 3a, Fig. 3b shows particle sizes (μm) from the VIIRS retrieval. Each red line segment from Fig. 3a is also superimposed on the plot of particle sizes for ease of comparison. As suggested by the image, cloud top particle sizes were smaller (approximately 3 to 6 μm) than those of nearby clouds (approximately 18 to 30 μm). A word of caution, however, should be exercised with the use of the values of the sizes of the cloud droplets from the retrieval.

[Figure 3]

Interpretation of the imagery shown in Fig.'s 1, 2, and 3 is consistent with the relationship between cloud properties and measured radiances discussed above. That

is, values of visible reflectance (as measured within bands I1, I2, and I3) increase with increasing optical depth and values of brightness temperature (as measured within band I4) increase with decreasing particle size. Therefore, all four bands suggest not only an increase in the number of cloud droplets, but also that the cloud droplets were smaller within the streaks compared to surrounding clouds. Similar to the formation of ship tracks, the addition of more aerosols, which act as condensation nuclei, from below the cloud layer could produce the streaks. In addition to S-NPP VIIRS, GOES-13 imagery also captured the streaks. A sequence of GOES-13 visible images of the event is displayed in Fig. 4, while a sequence of images at 3.9 μm is shown in Fig. 5. In both Figs. 4 and 5, images are shown approximately every two hours. In the first panel, at 1402 UTC, no streaks existed. Shortly thereafter, however, streaks became evident at 1602 UTC in both bands. In time, the streaks lengthened and exhibited a distinct contrast in reflectance (Fig. 4 c and d) and brightness temperature (Fig. 5 c and d). In each band, a stationary source appears on the northwest end of the streaks. The contrast between the streaks and surrounding clouds is greater in the 3.9 μm band than in the visible, suggesting that the difference is due more to cloud particle size variations than in optical depth variations.

[Figure 4]

[Figure 5]

One possible source of particulate matter is emissions from industrial smoke stacks. On this particular day, however, another source was the cause: prescribed

burning of slash from logging activity in the region**.** This conclusion was confirmed by the Ontario Ministry of Natural Resources, Aviation, Fire and Emergency Services-Northeast Region. They graciously provided the latitudes and longitudes (red stars in Fig.'s 1 and 3) of the slash burning that occurred on 28 October 2013. Logging slash from earlier harvesting operations is often piled, and then burned in late fall when lower fire danger conditions prevail, thus lessening the chance of fires escaping control. This has become a common practice in recent years; consequently, there exist two important issues related to this event. First, emissions from slash burning did alter the microphysical properties of low-level liquid water clouds. Secondly, all of the streaks can be used as an indirect means to identify the location of burning. As seen in Fig. 5, the actual hotspots from the majority of the fires are not evident due to the presents of clouds, but the altered cloud properties did allow the fire locations to be identified. In this case, the fires were prescribed burns, but a similar technique might be used to locate wildfires when low clouds prevent a view of the surface.

4. Summary

On the afternoon of 28 October 2013, over eastern Ontario, Canada, both S-NPP VIIRS and GOES-13 detected plume-like streaks in a low-level liquid water cloud field. These streaks were reminiscent of ship tracks that are common off the west coast of California. Like ship tracks, the streaks were brighter in the visible reflective bands and warmer in bands at 3.9 μm. Increased optical depth, as a result of the

increased cloud droplet number concentration, was responsible for the enhanced albedo in the visible bands while smaller cloud droplet size was responsible for increased brightness temperatures at 3.9 μm. Both effects were caused by a local increase of aerosols into the liquid water cloud layer.

Slash burning of logging debris was confirmed as the local source of aerosols. Similar to ship tracks, the additional aerosols lead to an increase in the number of smaller cloud particles. Two important consequences of this event are as follows: First, aerosols from slash burning did alter the microphysical characteristics of the clouds. This is similar not only to the impact of aerosols from ships on the overlaying marine stratocumulus layer, but also the significant source of aerosols from biomass burning associated with wildland fires on pyro-cumulonimbus. Secondly, in this case the low-level liquid water cloud field prevented the detection of the hotspots associated with the burning slash. However, the plume-like streaks in the cloud field indirectly identified the location and existence of fires. Due to the relatively small length scale of the plume-like streaks in the cloud field, detection may be best suited for an automated algorithm.

Acknowledgements

This research is primarily funded by NOAA's National Environmental Satellite, Data, and Information Service (NESDIS) GOES-R Program Office. We would also like to extend our thanks to Rene Servranckx (Environment Canada) and Mike Fromm (Naval Research Laboratory) for their assistance. Further thanks are extended to Natalie Belanger, Northeast Regional GIS Data Technician, Sudbury and Mike Jackson, Northeast Regional Fire Response Specialist, Sudbury. The views, opinions, and findings in this report are those of the authors, and should not be construed as an official NOAA and or U.S. Government position, policy, or decision.

References

Cheng, Y., Lohmann, U., Zhang, J., Luo, Y., Liu, Z., and Lesins, G. (2005), *Contributions of changes in sea surface temperature and aerosol loading to decreasing precipitation trend in Southern China*. J. Climate 18, 1381-1390

Fromm, M., Lindsey, D.T., Servranckx, R., Yue, G., Trickl, T., Sica, R., Doucet, P., Godin-Beekmann, S. (2010), *The Untold Story of Pyrocumulonimbus*. Bull. Amer. Meteor. Soc. 91:9, 1193–1209. doi: 10.1175/2010BAMS3004.1

Giglio, L., Kendall, J.D., and Mack, R. (2003), *A multi-year active fire dataset for the tropics derived from the TRMM VIRS*, Int. J. Remote Sens. 24, 4505–4525

Giglio, L., Loboda, T., Roy, D.P., Quayle, B., and Justice, C.O. (2009), *An active-fire based burned area mapping algorithm for the MODIS sensor*, *Remote Sens. Environ*. 113, 408–420, doi:10.1016/j.rse.2008.10.006

Hillger, D. W., and Schmit, T.J. (2009), *The GOES-13 science test: A synopsis*, Bull. Amer. Meteor. Soc. 90, 6-11

Hillger, D., Kopp, T., Lee, T., Lindsey, D., Seaman, C., Miller, S., Solbrig, J., Kidder, S., Bachmeier, S., Jasmin, T., and Rink, T. (2013), *First-Light imagery from Suomi NPP VIIRS,* Bull. Amer. Meteor. Soc. 94,1019-1029, doi:10.1175/BAMS-D-12-00097.1

Kaskaoutis, D.G., Kharol, S.K., Sifakis, N., Nastos, P.T., Sharma, A.R., Badarinath, K.V.S., and Kambezidis, H.D. (2011), *Satellite monitoring of the biomass-burning aerosols during the wildfires of August 2007 in Greece: Climate implications,* Atmospheric Environment 45, 716-726

Lindsey, D. T., and Fromm, M. (2008), *Evidence of the cloud lifetime effect from wildfire-induced thunderstorms*, Geophys. Res. Lett. 35, 22809,DOI:10.1029/2008GL035680

National Polar-Orbiting Operational Environmental Satellite System (NPOESS) Cloud Effective Particle Size and Cloud Optical Thickness Algorithm Theoretical Basis Document (ATBD) (D43750 Rev A), CDRL No. A032. (2010)

Platnick, S., Durkee, P.A., Nielsen, K., Taylor, J.P., Tsay, S.-C., King, M.D., Ferek, R.J., Hobbs, P.V., and Rottman, J.W. (2000), *The role of background cloud microphysics in the radiative formation of ship tracks*. J. Atmos. Sci. 57, 2607-2624

Prins, E.M., and Menzel, W.P. (1992), *Geostationary satellite detection of biomass burning in South America*, Int. J. Remote Sens. 13, 2783–2799

Prins, E.M., Feltz, J.M., Menzel, W.P., and Ward, D.E. (1998), *An overview of GOES-8 diurnal fire and smoke results for SCAR-B and 1995 fire season in South America*, J. Geophys. Res. 103(D24), 31,821– 1,835, doi:10.1029/98JD01720

Rosenfeld, D. (2000), *Suppression of rain and snow by urban and industrial air pollution*, Science 287, 1793-1796

Sifakis, N. I., and Iossifidis, C. (2014), *CHRISTINE Code for high resolution satellite mapping of optical thickness and angstrom exponent. Part I: Algorithm and code*, Computers and Geosciences 62, 136-141

Twomey, S. (1977), *The influence of pollution on the shortwave albedo of clouds*, J. Atmos. Sci. 34, 1149-1152

Weaver, J.F., Lindsey, D.T., Bikos, D.E., Schmidt, C.C., and Prins, E.M. (2004), *Fire Detection using GOES-11 Rapid Scan Imagery.* Wea. Forecasting 19, 496-510

Zhang, X., Kondragunta, S., Ram, J., Schmidt, C., and Huang, H.-C. (2012), *Near-real-time global biomass burning emissions product from geostationary satellite constellation, J. Geophys. Res*. 117, D14201, doi:10.1029/2012JD017459

Figures

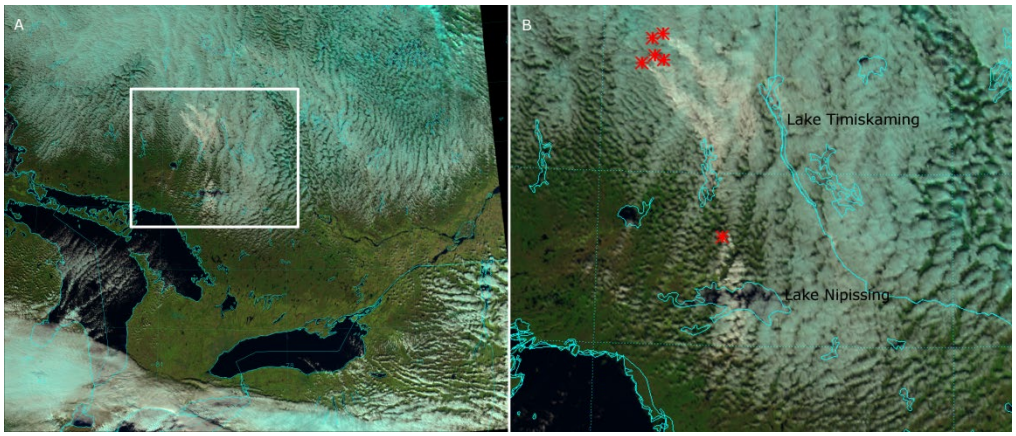

Figure 1: (A) Natural color composite from S-NPP VIIRS using bands I1 (0.64 μm), I2 (0.865 μm), and I3 (1.61 μm) over eastern Ontario, Canada on 28 October 2013 at 18:53 UTC. Bright plume-like streaks are evident in the region bounded by the white box. (B) Closer view of the region bounded by the white box in (A) with the latitude and longitude of the origin of each plume.

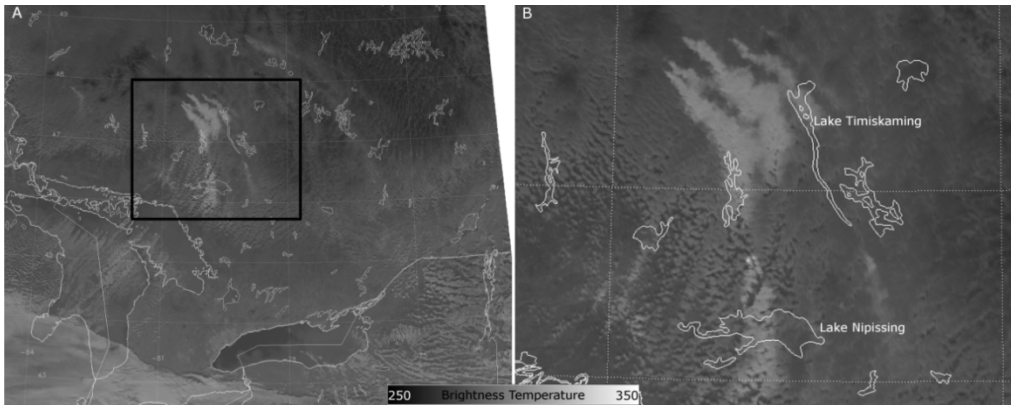

Figure 2: Same as Figure 1 except for band I4 (3.74 μm). In this imagery darker/lighter shades represent colder/warmer brightness temperatures.

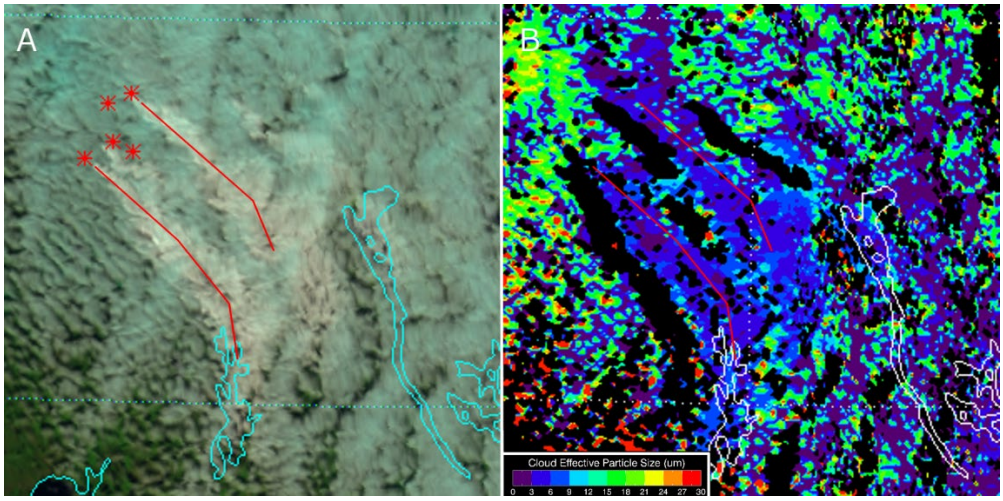

Figure 3: Close-up view of (A) the natural color image with red stars and line segments indicating the bright streaks and (B) VIIRS retrieved cloud droplet sizes (μm).

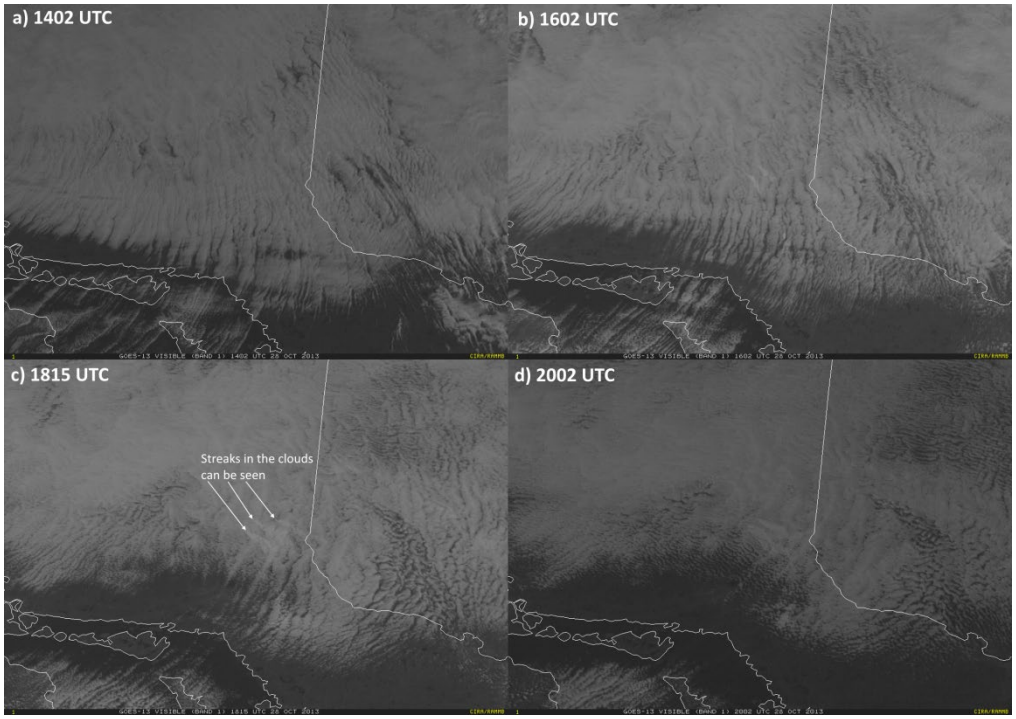

Figure 4: GOES-13 imagery at 0.67 μm on 28 October 2013 at (a) 1402, (b) 1602, (c) 1815, and (d) 2002 UTC.

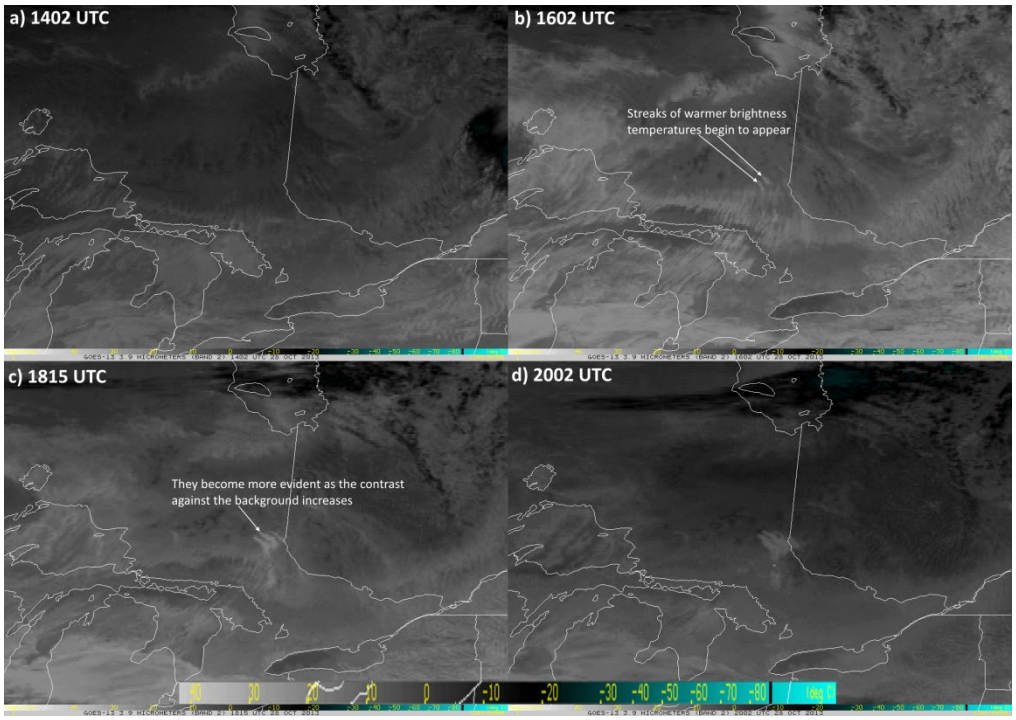

Figure 5: Same as Figure 4, but for GOES-13 imagery at 3.9 µm. A color table is displayed across the bottom of this figure to indicate brightness temperature (ºC).

Tables

Table 1: This table contains details of the first two bands on GOES-13 along with the first four I-bands on S-NPP VIIRS.

GOES Band	Central Wavelength (μm)	Band Width (μm)
1	0.65	0.55 – 0.75
2	3.9	3.80 – 4.00
VIIRS Band	Central Wavelength (μm)	Band Width (μm)
I1	0.64	0.60 – 0.68
I2	0.865	0.85 – 0.88
I3	1.61	1.58 – 1.64
I4	3.74	3.55 – 3.93